JCI The Journal of Clinical Investigation

Glucocorticoids paradoxically facilitate steroid resistance in T-cell acute lymphoblastic leukemias and thymocytes

Lauren K. Meyer, … , David T. Teachey, Michelle L. Hermiston

J Clin Invest. 2019. https://doi.org/10.1172/JCI130189.

Research In-Press Preview Oncology

Graphical abstract

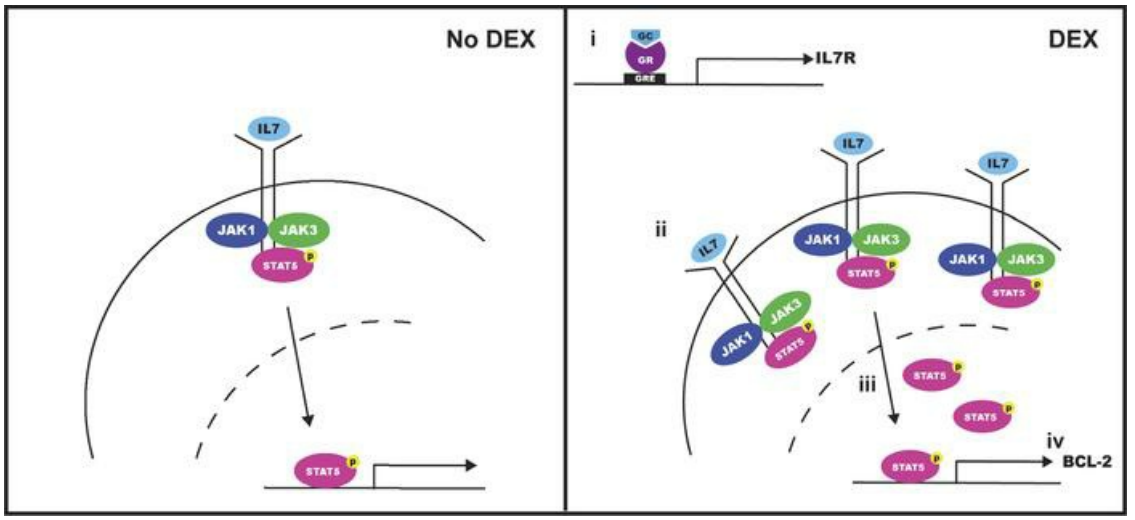

Glucocorticoids paradoxically facilitate steroid resistance in T-cell acute lymphoblastic leukemias and thymocytes

Authors: Lauren K. Meyer[1], Benjamin J. Huang[1], Cristina Delgado-Martin[1], Ritu P. Roy[2], Aaron Hechmer[2], Anica M. Wandler[1], Tiffaney L. Vincent[3], Paolo Fortina[4], Adam B. Olshen[2,5], Brent L. Wood[6], Terzah M. Horton[7], Kevin M. Shannon[1,2], David T. Teachey[3*], and Michelle L. Hermiston[1,2*]

Affiliations:

[1]Department of Pediatrics, University of California, San Francisco, CA, USA

[2]Helen Diller Family Comprehensive Cancer Center, San Francisco, CA, USA

[3]Department of Pediatrics, University of Pennsylvania, Philadelphia, PA, USA

[4]Cancer Genomics and Bioinformatics Laboratory, Sidney Kimmel Cancer Center, Thomas Jefferson University, Philadelphia, PA, USA

[5]Department of Epidemiology and Biostatistics, University of California, San Francisco, CA, USA

[6]Department of Laboratory Medicine and Pathology, University of Washington, Seattle, WA, USA

[7]Texas Children's Cancer and Hematology Centers, Baylor College of Medicine, Houston, TX, USA

*These authors contributed equally.

To whom correspondence should be addressed:

David Teachey: 3501 Civic Center Blvd., Philadelphia, PA, 19104. Teacheyd@email.chop.edu, (267) 426-0762

Michelle Hermiston: 550 16th Street, 4th Floor Mailstop 0434, San Francisco, CA, 94143. Michelle.hermiston@ucsf.edu, (415) 476-2413

The authors have declared that no conflict of interest exists.

Abstract

Glucocorticoids (GCs) are a central component of therapy for patients with T-cell acute lymphoblastic leukemia (T-ALL) and while resistance to GCs is a strong negative prognostic indicator in T-ALL, mechanisms of GC resistance remain poorly understood. Using diagnostic samples from patients enrolled on the frontline Children's Oncology Group (COG) T-ALL clinical trial AALL1231, we demonstrated that one-third of primary T-ALLs were resistant to GCs when cultured in the presence of interleukin-7 (IL7), a cytokine that is critical for normal T-cell function and that plays a well-established role in leukemogenesis. We demonstrated that in these T-ALLs and in distinct populations of normal developing thymocytes, GCs paradoxically induced their own resistance by promoting upregulation of IL7 receptor (IL7R) expression. In the presence of IL7, this augmented downstream signal transduction resulting in increased STAT5 transcriptional output and upregulation of the pro-survival protein BCL-2. Taken together, we demonstrated that IL7 mediates an intrinsic and physiologic mechanism of GC resistance in normal thymocyte development that is retained during leukemogenesis in a subset of T-ALLs and is reversible with targeted inhibition of the IL7R/JAK/STAT5/BCL-2 axis.

Introduction

T-cell acute lymphoblastic leukemia (T-ALL) is a genetically heterogeneous disease characterized by a range of alterations involving transcription factors, cell cycle regulators, and signal transduction effectors (1). Unlike B-cell ALL (B-ALL), where genetic factors are widely used to inform risk stratification and subsequent intensification of therapy (2), few genetic lesions in T-ALL have independent prognostic significance (1). As a result, efforts to implement risk-adapted therapeutic strategies have been limited by a lack of genetic biomarkers, highlighting the need for functional studies aimed instead at elucidating recurrent patterns of drug response and resistance across the spectrum of T-ALL.

While outcomes for children with T-ALL have improved dramatically over the past several decades, children with relapsed T-ALL continue to face poor survival rates (3), suggesting that novel strategies are needed to improve the upfront efficacy of therapy in order to induce deeper remissions and decrease the likelihood of disease relapse. Glucocorticoids (GCs) are a central component of T-ALL therapy, and the initial response to GC therapy is an important predictor of long-term outcomes (4). For example, on the ALL-BFM 95 trial, patients were stratified into those who had a prednisone good response (PGR) and those who had a prednisone poor response (PPR) following seven days of prednisone monotherapy. Patients with a PGR had an eight-year event free survival rate of 81.3%, as opposed to only 55.1% for patients with a PPR (5). These data demonstrate that intrinsic differences in GC sensitivity exist at the time of disease diagnosis and that these differences can have long-term prognostic significance. Despite decades of clinical use, a comprehensive understanding of the mechanistic basis for differential intrinsic GC sensitivity is lacking. GCs act by binding to a cytoplasmic GC receptor (GR), which promotes translocation of GR to the nucleus where it binds to target gene loci and induces a transcriptional program that results in apoptosis in lymphoid cells (6). Unlike other agents used in the treatment of T-ALL, GCs are unique in that they also exist as endogenous hormones that play critical roles in normal T-cell physiology. For example, endogenous GC activity has been shown to interact with T-cell receptor (TCR) signaling to shape the developing T-cell repertoire (7, 8) and to promote T-cell homeostasis in the periphery following an immune response (9). Given these frequent

encounters with GCs in normal physiology and the fact that GCs are potent inducers of apoptosis in both normal and transformed lymphoid cells, we reasoned that T-cells must possess intrinsic mechanisms that allow them to resist GC-induced apoptosis under certain developmental and environmental conditions. Furthermore, we hypothesized that these mechanisms may be retained during leukemogenesis and exploited to confer resistance to GC therapy in T-ALL.

One critical endogenous factor in the T-ALL microenvironment is the cytokine interleukin-7 (IL7). In addition to promoting the survival and differentiation of developing thymocytes (10), the IL7 receptor (IL7R)/JAK/STAT5 signaling pathway contributes to T-ALL pathogenesis and disease maintenance (11–13). We previously demonstrated that over half of primary treatment-naïve T-ALL patient samples are intrinsically resistant to the glucocorticoid dexamethasone (DEX) when cultured in the presence of IL7. Of these DEX resistant samples, half could be sensitized to DEX with inhibition of JAK signaling (14). Interestingly, the majority of samples with JAK/STAT5-mediated DEX resistance lacked activating mutations in components of the IL7R/JAK/STAT5 pathway. In the present study, we analyzed a larger cohort of fresh diagnostic samples obtained from pediatric patients enrolled on the COG frontline T-ALL clinical trial AALL1231, with the goal of establishing the mechanistic basis for this DEX resistance phenotype. In this cohort, we demonstrated that one-third of primary diagnostic samples are resistant to DEX specifically when cultured in the presence of IL7. Furthermore, we found that subsets of normal developing thymocytes similarly demonstrate this IL7-induced DEX resistance phenotype. Through functional analyses, we elucidated a mechanism by which GCs paradoxically induce their own resistance by augmenting the pro-survival activity of the IL7R/JAK/STAT5 pathway in distinct subsets of developing thymocytes and T-ALLs. Taken together, these data suggest that IL7 facilitates GC resistance in developing thymocyte populations, and that subsets of T-ALL cells retain this capacity to utilize IL7 as a means of resisting GC-induced apoptosis. These findings have significant therapeutic implications, as they suggest that inhibiting the IL7R/JAK/STAT5 pathway or its transcriptional targets may enhance GC efficacy in patients who exhibit a poor initial response to GC therapy.

Results

JAK signaling mediates dexamethasone resistance in a subset of T-ALLs

In a large independent cohort consisting of 73 samples from patients enrolled on COG AALL1231, we validated our previous finding that in vitro DEX sensitivity is highly variable across T-ALL (Figure 1A) (14). Importantly, these differences in DEX sensitivity are not dose-dependent, but persist at saturating concentrations of DEX (Figure S1A). Defining “DEX resistant” as samples that retain greater than 50% cell viability following DEX exposure, we found that 63% of primary diagnostic samples are intrinsically DEX resistant when cultured in the presence of IL7 (Figure 1A). Binding of IL7 to IL7R results in the recruitment of JAK1 and JAK3, which subsequently become phosphorylated to create docking sites for STAT5 (15). Consistent with our previous findings (14), inhibition of JAK signaling with the JAK1/2 inhibitor ruxolitinib (RUX) was sufficient to overcome DEX resistance in 54% of these DEX resistant samples ($p<0.0001$ for DEX versus DEX+RUX and for RUX versus DEX+RUX; Figure 1B).

To facilitate further studies aimed at investigating the mechanistic basis for DEX resistance mediated by JAK signaling, we next evaluated the human T-ALL cell line CCRF-CEM for its utility as a model system in which to study the DEX resistance phenotype observed in these primary patient T-ALL samples. This analysis revealed a dose-dependent reduction in DEX sensitivity with increasing concentrations of IL7 (Figures 1C and S1B). Consistent with the primary patient samples, RUX was sufficient to completely restore DEX sensitivity in CCRF-CEM cells in the presence of IL7 (Figure 1D). Furthermore, Bliss independence analysis indicated a synergistic interaction between DEX and RUX (Figure 1E). To ensure that this sensitization effect was due specifically to JAK1 inhibition by RUX and not to off-target effects, we also utilized the JAK3 inhibitor tofacitinib, which should similarly inhibit IL7R signaling, and the JAK2 inhibitor CHZ868, which should not inhibit IL7R signaling. In this analysis, tofacitinib phenocopied the effects of RUX to overcome IL7-induced DEX resistance while CHZ868 had no effect on cell viability (Figure S1C), suggesting that on-target inhibition of JAK1 or JAK3 is sufficient to abrogate IL7-induced DEX resistance.

Dexamethasone exposure augments IL7R/JAK/STAT5 pathway activity

To confirm that IL7 induces DEX resistance in CCRF-CEM cells via signaling through IL7R, we first used CRISPR/Cas9 genome editing to generate clonal populations of scramble control and IL7Rα knockout (KO) CCRF-CEM cells (Figure S2A). In the KO clones, loss of IL7Rα expression was sufficient to restore DEX sensitivity in the presence of IL7 (Figure 2A). We next asked whether IL7R signaling interferes with the activation and/or function of GR. First, to determine whether exposure to IL7 alters the availability of GR for DEX binding, we assessed GR protein expression in CCRF-CEM cells treated with DEX with or without IL7. Under these conditions, DEX exposure effectively induced GR expression to comparable levels regardless of the presence of IL7 (Figure S2B). Furthermore, upon exposure to DEX both in the absence and presence of IL7, GR effectively translocated to the nucleus and became phosphorylated on Ser211 (Figure S2C), a modification that has been shown to correlate with the capacity to activate or repress transcription (16). Finally, to determine whether IL7 interferes with induction of the GR transcriptional program, we performed RNA sequencing (RNA-seq) on four scramble control CCRF-CEM cell clones exposed to vehicle control or DEX with or without IL7 for four hours to elucidate primary GR target genes. Under these conditions, IL7 did not interfere with GR-mediated transcript induction or repression (Figure S2D and Table S1). Taken together, these data suggest that GR activity remains intact in the presence of IL7.

In some mature T-cell populations, GCs have been shown to induce expression of IL7Rα (17–20). Specifically, chromatin immunoprecipitation (ChIP) studies in both murine (21) and human (22) lymphocytes have demonstrated that GR is recruited to a GR binding motif in a noncoding sequence upstream of the IL7Rα promoter, and deletion of this region is sufficient to abrogate GR-induced upregulation of IL7Rα (17), suggesting that IL7Rα upregulation occurs as a direct transcriptional effect of activated GR. To determine if DEX modulates IL7Rα expression in CCRF-CEM cells, we measured *IL7RA* transcript before and after DEX exposure and found a time-dependent increase in *IL7RA* transcript expression (Figure 2B) that occurred both in the absence and presence of IL7 (Figure S2E). DEX exposure also increased IL7Rα protein expression at the cell surface relative to untreated cells ($p<0.0001$). This increase was inhibited in the presence of the translation inhibitor cycloheximide

(CHX), suggesting that the increase in cell surface IL7Rα reflects *de novo* protein synthesis rather than re-localization of existing protein (Figure 2C). Given our finding that inhibition of JAK signaling is sufficient to sensitize cells to DEX in the presence of IL7, we next asked whether the increase in cell surface IL7Rα expression is associated with an increased capacity for JAK signaling downstream of IL7R. We first exposed CCRF-CEM cells to DEX for 24 hours, then stimulated them with IL7 and measured the induction of phosphorylated STAT5 (pSTAT5) as a downstream effector of JAK signaling (Figure S2F). Under these conditions, DEX exposure resulted in significantly more robust pSTAT5 induction in response to IL7 stimulation relative to untreated cells ($p=0.0002$). Furthermore, pre-treating these cells with RUX for one hour prior to IL7 stimulation was sufficient to abrogate the increased JAK/STAT5 signaling following DEX exposure (Figures 2D and S2G). Importantly, IL7 stimulation, either with or without DEX pre-treatment, did not induce phosphorylation of other STAT proteins that are activated downstream of other γ chain cytokine receptors (Figure S2H). Given this specific increase in STAT5 activation upon IL7 stimulation following DEX exposure, we then asked whether the increase in IL7Rα expression is associated with a sustained increase in STAT5 transcriptional activity. To test this, we transiently transfected CCRF-CEM cells with a STAT5-luciferase reporter construct and assessed STAT5-induced luciferase activity in cells exposed to DEX in the presence or absence of IL7 for 36 hours. This analysis revealed a significant induction of STAT5 transcriptional activity in cells exposed to the combination of DEX and IL7 relative to either DEX or IL7 alone ($p<0.0001$ versus both DEX alone and IL7 alone). Furthermore, the addition of RUX was sufficient to overcome this increase in transcriptional activity (Figure 2E). To further confirm this increase in STAT5 transcriptional output, we performed RNA-seq on scramble control CCRF-CEM cell clones treated with DEX with or without IL7 for four hours. Using gene set enrichment analysis (GSEA) with gene sets derived from published STAT5 ChIP with sequencing (ChIP-seq) data in human CD4+ T-cells (23), we found enrichment for transcriptional targets of STAT5A and STAT5B ($p<0.0001$; FDR<0.0001), STAT5A alone ($p=0.002$; false discovery rate (FDR)=0.001), and STAT5B alone ($p<0.0001$; FDR=0.001) in cells exposed to DEX plus IL7 relative to IL7 alone (Figure 2F and Table S2), further supporting the finding that, in the presence of IL7, DEX exposure augments activation of the STAT5 transcriptional program.

BCL-2 is a critical mediator of IL7-induced dexamethasone resistance

Based on these findings, we hypothesized that STAT5 may be an important downstream mediator of DEX resistance in the presence of IL7. To directly interrogate the role of STAT5 in this context, we used CRISPR/Cas9 genome editing to generate clonal populations of STAT5A KO, STAT5B KO, and STAT5A/B double KO CCRF-CEM cells (Figure 3A). Importantly, deletion of one or both STAT5 isoforms did not affect expression of GR relative to scramble control clones (Figure S3A). Exposure of STAT5 KO cells to DEX in the presence or absence of IL7 revealed that deletion of STAT5B, but not of STAT5A, was sufficient to significantly attenuate DEX resistance in the presence of IL7 (Figures 3B and S3B). These data suggest that transcriptional targets of STAT5B represent candidate DEX resistance genes. To identify these candidate genes, we performed RNA-seq on scramble control and STAT5A/B KO CCRF-CEM cell clones treated with DEX with or without IL7 for sixteen hours. Using these data, we found that deletion of STAT5A/B did not affect the capacity for DEX-induced upregulation of *IL7RA* (Figure S3C), further confirming that IL7R upregulation is a GR-dependent but STAT5-independent transcriptional event. Using differential expression analysis, we identified the top differentially expressed genes between scramble control cells treated with DEX alone or with the combination of DEX and IL7 (Table S3). We then compared this gene list to the core enrichment genes from the STAT5B gene set (Figure 2F and Table S2) to identify STAT5B target genes that are differentially expressed in cells exposed to DEX relative to the combination of DEX and IL7. This analysis identified the anti-apoptotic family member *BCL2* (log fold change = 1.48 for DEX+IL7 relative to DEX alone) and the Rho guanine nucleotide exchange factor *ARHGEF3* (log fold change = 1.64) as two candidate mediators of DEX resistance in the presence of IL7 (Figure 3C). Consistent with their presence on both of these gene lists, targeted analysis of the RNA-seq data revealed that these genes were induced by the combination of DEX and IL7 relative to DEX or IL7 alone only in the scramble control clones and not in the STAT5A/B KO clones (Figures 3D and 3E).

Given the anti-apoptotic function of BCL-2 and the importance of downregulation of BCL-2 for DEX-induced apoptosis in T-ALL cells (24), we focused subsequent analyses on BCL-2 expression and

function. Interestingly, other anti-apoptotic BCL-2 family members were not regulated in a similar manner in response to DEX and IL7 (Figure S3D), suggesting a BCL-2-specific effect. To determine whether the induction of BCL-2 expression upon exposure to DEX and IL7 is mediated specifically by STAT5B, we assessed BCL-2 protein expression in scramble control and STAT5 single and double KO CCRF-CEM cell clones. This analysis revealed upregulation of BCL-2 with the combination of DEX and IL7 in scramble control and STAT5A single KO clones, but not in either the STAT5B single KO or STAT5A/B double KO clones, consistent with a central role for STAT5B in the regulation of BCL-2 expression (Figures 3F and S3E).

Given that this increased STAT5 transcriptional activity depends first on the upregulation of IL7Rα as a primary transcriptional target of GR, we reasoned that STAT5-mediated upregulation of BCL-2 must occur as a secondary transcriptional effect following exposure to DEX and IL7. To test this, we performed qPCR to measure the changes in expression over time of *BCL2* and of primary GR target genes in CCRF-CEM cells cultured in the presence of DEX and IL7. This analysis revealed that while primary GR transcriptional targets are upregulated as early as two hours following DEX treatment, *BCL2* is not significantly upregulated until the eight-hour time point (Figure S3F). To further confirm that *BCL2* is upregulated as a secondary transcriptional target, we exposed CCRF-CEM cells to DEX with or without IL7 in the presence or absence of CHX and measured transcript and protein expression of *BCL2* and of the primary GR transcriptional target *BCL2L11* (BIM) (24). CHX was sufficient to inhibit the upregulation of BIM and BCL-2 protein expression, suggesting effective inhibition of translation and *de novo* protein synthesis (Figure S3G). *BCL2L11* transcript expression was induced by DEX both in the absence and presence of CHX, consistent with this being a primary transcriptional target of GR, the upregulation of which is not dependent on intermediary *de novo* protein synthesis. In contrast, *BCL2* transcript expression was upregulated only in the absence of CHX, suggesting a dependence on *de novo* protein synthesis, consistent with this being a secondary transcriptional event (Figure 3G).

To establish the functional significance of BCL-2 upregulation, we first performed BH3 profiling with the BCL-2 inhibitor ABT-199 in CCRF-CEM cells treated with DEX with or without IL7. Under these conditions, DEX alone produced a significant increase in apoptotic priming ($p=0.0007$). This effect was

attenuated in the presence of IL7 (p=0.64), suggesting that the increase in BCL-2 expression with the combination of DEX and IL7 is sufficient to oppose the induction of the apoptotic program (Figure 4A). To determine whether ABT-199 may have a therapeutic role to enhance DEX sensitivity in the presence of IL7, we exposed CCRF-CEM cells to DEX in the presence of IL7 and increasing concentrations of ABT-199. This analysis demonstrated that ABT-199 potently sensitizes cells to DEX in the presence of IL7 in a synergistic manner (Figures 4B and 4C)**.** In addition, we utilized a series of short hairpin RNAs (shRNAs) to knock down BCL-2 expression in CCRF-CEM cells and found that loss of BCL-2 expression increases sensitivity to DEX in the presence of IL7 in a manner that correlates with the degree of BCL-2 knockdown (Figures S4A and 4D-E). To assess the importance of high BCL-2 expression in a patient cohort for which clinical outcome data are available, we next analyzed published gene expression data from 265 diagnostic T-ALL samples obtained from patients enrolled on the prior COG T-ALL trial AALL0434 (1). Consistent with our in vitro findings, we found that patients who were minimal residual disease (MRD) positive at the end of induction therapy had significantly higher BCL-2 expression relative to patients who were MRD negative (p=0.0009 for patients with MRD <1% and p<0.0001 for patients with MRD >1%; Figure 4F), suggesting a relationship between high BCL-2 expression and relative GC resistance. In contrast, shRNA-mediated knockdown of the other candidate resistance gene, *ARHGEF3*, had no effect to overcome IL7-induced DEX resistance (Figures S4B-C) and *ARHGEF3* expression did not differ according to MRD status in the AALL0434 patient cohort (Figure S4D). Taken together, these data support a model (Figure 4G) whereby DEX (i), through upregulating IL7Rα expression (ii), paradoxically induces its own resistance by augmenting JAK/STAT5 signaling (iii) and activation of STAT5B target genes (iv), including *BCL2*. This upregulation of BCL-2 in turn is sufficient to antagonize the pro-apoptotic effects of DEX.

IL7 induces dexamethasone resistance in subsets of developing thymocytes

We next sought to determine why IL7-mediated DEX resistance occurs only in a subset of primary patient T-ALL samples. In our previous patient cohort, we demonstrated that 64% of samples with IL7-mediated DEX resistance did not have activating mutations in the IL7R/JAK/STAT5 pathway

(14), suggesting that this phenotype is not dictated by the mutational status of a T-ALL sample. Given these findings, an alternative hypothesis is that IL7-mediated DEX resistance might reflect a physiologic mechanism of GC resistance that occurs in normal populations of developing thymocytes, as both GC sensitivity and IL7R expression are known to vary throughout development (10, 25). To test this hypothesis, we evaluated normal murine thymocytes to determine if IL7R/JAK/STAT5 signaling modulates DEX sensitivity. We first exposed mice to DEX in vivo and assessed the relative sensitivity of the major thymocyte subpopulations. In this analysis, DEX induced a significant reduction in overall thymic cellularity ($p=0.02$; Figure S5A) and resulted in a dramatic shift in the distribution of the major thymocyte subpopulations. Consistent with previous reports (25), we found that DEX induced a significant reduction in the proportion of CD4/CD8 double positive (DP) thymocytes ($p<0.0001$), with a compensatory increase in the percentage of the earlier double negative (DN) thymocytes ($p=0.005$) and later single positive (SP) thymocytes ($p<0.0001$ for both CD4 and CD8 SP thymocytes; Figures 5A, S5B, and S5C). Importantly, we recapitulated the findings by other investigators (26) that GR expression is paradoxically lowest at the DP stage of development despite these cells being highly DEX sensitive, suggesting that GR expression is insufficient to explain this pattern of differential sensitivity (Figure S5D). To determine if this differential DEX sensitivity reflects differences in the apoptotic potential of these thymocyte subpopulations in their basal state, we performed BH3 profiling on freshly harvested thymocytes. We found that DP thymocytes have significantly higher apoptotic potential relative to DN or SP thymocytes ($p=0.002$, $p=0.0004$, and $p=0.01$ versus DN, CD4 SP, and CD8 SP thymocytes, respectively; Figure 5B), consistent with the pattern of DEX sensitivity observed in vivo.

We next evaluated basal IL7Rα expression and signaling capacity across the major thymocyte subpopulations. Consistent with previous reports (10), we found a reduction in IL7Rα expression and IL7-induced pSTAT5 in the DP thymocytes relative to the DN and SP thymocytes (Figures 5C and 5D). Based on these findings and the pattern of DEX sensitivity we observed in vivo, we hypothesized that the presence of IL7 in the in vivo microenvironment might activate JAK/STAT5 signaling in DN and SP thymocytes, which could in turn confer protection against the GC surges that occur during a physiologic stress response (27) and against pharmacologic concentrations of GCs. To test this hypothesis, we first

exposed thymocytes to vehicle or DEX ex vivo in the absence or presence of increasing concentrations of IL7. DN and SP thymocytes demonstrated profound DEX resistance specifically in the presence of IL7, while DP thymocytes remained highly sensitive to DEX regardless of IL7 (Figure 5E), consistent with their reduced IL7Rα expression (Figure 5C). To determine whether the mechanism of JAK/STAT5-mediated DEX resistance that we elucidated in CCRF-CEM cells is applicable in these thymocyte subpopulations, we exposed thymocytes to DEX ex vivo and assessed cell surface IL7Rα expression and BCL-2 expression. Consistent with the observed pattern of DEX resistance in the presence of IL7, DN and SP thymocytes significantly upregulated both IL7Rα expression ($p<0.0001$ for DN, CD4 SP and CD8 SP thymocytes; Figure 5F) and BCL-2 expression ($p=0.01$, $p=0.0005$, and $p=0.001$ for DN, CD4 SP, and CD8 SP thymocytes, respectively; Figure 5G) following exposure to DEX in the presence of IL7. Finally, to determine if this mechanism is applicable in vivo under normal physiologic conditions, we treated mice with DEX and assessed BCL-2 protein expression in the major thymocyte subpopulations. DN and CD4 SP thymocytes, but not DP thymocytes, significantly upregulated BCL-2 expression in response to DEX ($p=0.007$ and $p=0.004$ for DN and CD4 SP thymocytes, respectively; Figure 5H). Finally, to determine whether human thymocytes demonstrate a similar pattern of IL7Rα expression and IL7-induced DEX resistance throughout development, we performed ex vivo analysis of healthy human thymocytes. Similar to the pattern observed in murine thymocytes, DN and SP thymocytes had the most significant increase in cell surface IL7Rα expression following exposure to DEX (Figure S5E) and had the most profound IL7-induced DEX resistance (Figure S5F).

Developmental stage correlates with IL7-induced dexamethasone resistance in T-ALL

To further address the hypothesis that IL7R/JAK/STAT5-mediated DEX resistance may be retained from normal thymocyte development in a subset of T-ALLs, we performed RNA-seq on 76 primary diagnostic T-ALL samples from patients enrolled on COG AALL1231. Using a gene set derived from a comparison of early versus late developing thymocytes (28), we performed unbiased hierarchical clustering of these patient samples to classify samples as developmentally “early” or “late” (Figure 6A). We next performed detailed in vitro analysis of 15 of the early T-ALL samples and 12 of the

late T-ALL samples isolated from patient derived xenografts (PDXs). Additional information about these samples is presented in Table S4. There were no differences in basal GR expression between these two groups (Figure S6A). Upon analysis of cell surface IL7Rα expression, we found that the early samples tended to have higher basal IL7Rα expression and a more robust induction of IL7Rα upon exposure to DEX (Figure 6B). This higher basal IL7Rα expression was also associated with an increased response to IL7 stimulation, as measured by pSTAT5 (Figure S6B). Consistent with this finding, only the early sample group demonstrated a significant increase in DEX resistance in the presence of IL7 ($p=0.0007$ and $p=0.69$ for early and late samples, respectively; Figure 6C). To determine whether this resistance phenotype was associated with activating mutations in the IL7R/JAK/STAT pathway, we performed variant calling using the RNA-seq data and found no enrichment for IL7R pathway mutations in the early samples (Figure S6C and Table S5), consistent with our previous analysis (14). Similar to the findings in CCRF-CEM cells, these early samples demonstrated an increase in BCL-2 protein expression in the presence of IL7, which was further augmented upon concomitant exposure to DEX and attenuated with the addition of RUX (Figure 6D). Moreover, both RUX and ABT-199 significantly sensitized early T-ALL samples to DEX in the presence of IL7 ($p<0.0001$ and $p=0.0005$ for the addition of RUX or ABT-199, respectively, to DEX plus IL7; Figure 6E). To evaluate the utility of RUX for overcoming DEX resistance in vivo in a preclinical model, we transplanted mice with early T-ALL T24 and treated them with DEX with or without RUX, using survival as the primary endpoint. As we observed in vitro (Figure S6D), the combination of DEX and RUX demonstrated increased in vivo efficacy relative to either agent alone ($p=0.003$ for RUX versus DEX+RUX and $p=0.02$ for DEX versus DEX+RUX; Figure 6F).

Discussion

The poor survival rates observed in children with relapsed T-ALL (3) suggest a need for strategies to enhance the efficacy of upfront therapy as a means of improving cure rates by decreasing the likelihood of disease relapse. While many studies have focused on understanding mechanisms of acquired drug resistance that arise during T-ALL treatment (29), the goal of our current study was instead to elucidate mechanisms of intrinsic drug resistance that dictate the initial response to therapy. In particular, the prognostic significance of the initial GC response in T-ALL (4) suggests a need for a deeper understanding of the mechanisms governing intrinsic differences in GC sensitivity. Here we demonstrate that functional analysis of a large number of diagnostic patient samples reveals recurrent patterns of intrinsic GC resistance across this otherwise genetically heterogeneous patient population. We confirm in this validation cohort that over half of the diagnostic T-ALL samples analyzed exhibit intrinsic DEX resistance in vitro, which has in turn been shown to correlate with clinical outcomes (30). Furthermore, we show that within this subset, half of the samples are resistant to DEX specifically in the presence of IL7.

Our data support a model whereby GCs paradoxically induce their own resistance by upregulating IL7Rα expression. In the presence of IL7, this leads to increased downstream signal transduction and STAT5 transcriptional output. This ultimately results in the upregulation of BCL-2, which is sufficient to counteract the pro-apoptotic effect of DEX. Given the prevalence of this phenotype, our data suggest that a significant percentage of T-ALL patients may benefit from the upfront addition of JAK or BCL-2 inhibitors as a means of improving the efficacy of GC therapy. Furthermore, we demonstrate the synergistic potential of combining DEX with these agents, suggesting that combination therapy may allow for a reduction in DEX dosing, thereby minimizing the numerous acute and chronic toxicities associated with steroid exposure (31) while simultaneously maximizing efficacy. In addition, our data demonstrate that STAT5B is primarily responsible for the upregulation of BCL-2 expression in this context, consistent with previous reports demonstrating that knockdown of STAT5A is insufficient to modulate IL7-mediated regulation of BCL-2 expression (11). Interestingly, this is also consistent with the finding that activating mutations in *STAT5B*, but not in *STAT5A*, commonly

occur in T-ALL *(1)*. These data support further investigation of the use of ABT-199 as a rational therapeutic strategy to enhance the efficacy of DEX in patients with *STAT5B*-mutated T-ALL.

In addition to mediating GC resistance in over one-third of diagnostic T-ALL samples, we demonstrate that IL7 similarly induces GC resistance in those populations of normal thymocytes in which IL7R signaling is important for survival and proliferation (10). Developing thymocytes are continuously exposed to endogenous GCs, but we and others (25) demonstrate that susceptibility to GC-induced apoptosis is variable over the course of thymocyte development. These data suggest that normal thymocyte populations must possess intrinsic mechanisms of GC resistance at distinct stages of development and/or under certain environmental conditions. In particular, we find that IL7-induced DEX resistance occurs in DN thymocytes and is enriched in T-ALL samples with an “early thymocyte” gene expression signature. Importantly, these early thymocytes undergo gene rearrangement to generate a fully rearranged TCR, which will be tested for functionality and auto-reactivity in the subsequent DP stage, a key process in the generation of mature functional T-cells (10). Teleologically, susceptibility to GC-induced apoptosis would be maladaptive early in development, as it would limit the availability of cells for this selection process. Our data therefore suggest that IL7-induced GC resistance may protect these early thymocyte populations from apoptosis in the presence of endogenous GCs. Furthermore, we demonstrate that this mechanism of intrinsic resistance is retained in T-ALLs resembling early thymocytes, where it may be exploited to enable resistance to pharmacologic concentrations of GCs.

Taken together, our data provide strong rationale for the idea that differential sensitivity to GC therapy at the time of disease diagnosis reflects developmentally programmed mechanisms of intrinsic GC resistance that are retained during the process of leukemogenesis. This work supports further studies aimed at elucidating additional mechanisms of GC resistance at distinct stages of thymocyte development as a means of understanding the factors that contribute to intrinsic GC resistance in T-ALL.

Methods

Patient samples and patient derived xenografts

Diagnostic blood samples were obtained from patients enrolled on the COG trial AALL1231. Immunophenotyping was performed and reviewed by immunophenotyping experts in COG. To establish patient derived xenografts, cells were injected into NOD/SCID/*Il2rg*^{tm1wjl}/Szj (NSG) mice obtained from Jackson Laboratories. Engraftment was monitored using flow cytometric analysis of peripheral blood with antibodies against human CD45 (BD Biosciences; 560973) and CD7 (BioLegend; 343105).

CCRF-CEM cells

CCRF-CEM cells were purchased from the UCSF Cell Culture Facility (ATCC CCL-119). Cells were authenticated via short tandem repeat DNA profiling and were routinely tested for mycoplasma contamination using the PlasmoTest detection kit (InvivoGen).

Preclinical trial

Five five-week-old male NSG mice per treatment arm were randomized to receive vehicle control, DEX, RUX, or the combination of DEX and RUX once the peripheral blood blast count reached 1%. RUX was administered in chow form (Incyte) continuously over the trial duration. DEX (Fresenius Kabi and Children's Hospital of Philadelphia Pharmacy) was administered at 7.5g/day by intraperitoneal injection. Mice were euthanized when they became moribund.

In vivo dexamethasone treatment in C57BL/6x129Sv/Jae mice and isolation of human and murine thymocytes

Six to eight-week-old male F1 C57BL/6x129Sv/Jae mice were obtained from the University of California, San Francisco Laboratory Animal Resource Center (LARC) breeding core. Mice were treated with 2mg/kg dexamethasone sodium phosphate (NDC 63323-516-10; University of California, San Francisco pharmacy) or vehicle control (phosphate buffered saline) once daily for three days.

Healthy human thymocytes were obtained from children undergoing cardiothoracic surgery at the University of California, San Francisco. Antibodies against murine CD4 (BioLegend; 100425) and CD8 (BioLegend; 100707) or human CD4 (Biolegend; 317420) or CD8 (BioLegend; 344706) were used to identify thymocyte subpopulations.

In vitro viability assays

In vitro viability assays were performed by exposing cells to vehicle control or dexamethasone (Sigma; D4902), ruxolitinib (Selleckchem; S1378), tofacitinib (Selleckchem; S5001), CHZ868 (MedKoo; 407137), or ABT-199 (ApexBio; A8194) for 72 hours (CCRF-CEM cells), 48 hours (PDX cells), or 24 hours (thymocytes) with or without recombinant human or murine IL7 (Peprotech; 200-07 and 217-17). Cells were then stained with Hoechst 33258 (Molecular Probes; H3569) and analyzed by flow cytometry.

CRISPR/Cas9 genome editing of CCRF/CEM cells

Cas9 protein containing a nuclear localization signal (Cas9-NLS) was purchased from the QB3 MacroLab at the University of California, Berkeley. Trans-activating CRISPR RNA (tracrRNA) and single guide RNAs (sgRNAs) were purchased from Dharmacon. sgRNA sequences targeting IL7Rα, STAT5A, and STAT5B were obtained from the Brunello sgRNA library (32) and are as follows: IL7Rα – AAAGAGCAATATATGTGTGA; STAT5A – ACATTCTGTACAATGAACAG; STAT5B – GTTCATTGTACAATATATGG. The scramble control cells were generated using a non-targeting sgRNA: GGTTCTTGACTACCGTAATT.

Ribonucleoproteins were prepared according to established methods (33). Electroporation was performed using the Amaxa Cell Line Nucleofector Kit C (Lonza, VACA-1004) and an Amaxa Nucleofector II Device with the electroporation code X-001. Editing was assessed by PCR amplification using the following primers: IL7Rα forward – 5'-TGAACATGCCTCCACTCACC-3'; IL7Rα reverse – 5'-CACACCTGGGTTTGAAGATCC-3'; STAT5A forward – 5'- TGGGGATAGTTCCTGAGGCT-3'; STAT5A reverse – 5' TGCCACCTCTTACACTTGCC-3'; STAT5B forward – 5'- TGTGCCCCTTAGGATGAAGC-

3'; STAT5B reverse – 5'- AATCACAGGAGGCACTGTTCC-3'. The amplicons were Sanger sequenced and the sequencing traces were analyzed using the TIDE analysis software (34). Clonal populations were generated using limiting dilution cell plating.

Western blotting

For analysis of protein expression in whole cell lysates, CCRF-CEM cells were resuspended in RIPA buffer. For analysis of cytoplasmic and nuclear protein, protein fractions were generated using the NE-PER kit (ThermoFisher Scientific; 78833). Immunoblotting was performed with the following antibodies: STAT5A (Abcam; ab32043), STAT5B (Abcam; ab178941), GR (Cell Signaling Technology; 12041), GR pS211 (Cell Signaling Technology; 4161), β-actin (Cell Signaling Technology; 3700), and p84 (Genetex; GTX70220). Donkey anti-rabbit IRDye800 and donkey anti-mouse IRDye680 secondary antibodies (LI-COR Biosciences) were used and imaging was performed using the Odyssey Imaging System (LI-COR Biosciences).

Quantitative PCR (qPCR)

CCRF-CEM cells were cultured in the presence or absence of 1μM DEX, 100ng/mL IL7, and/or 10μg/mL cycloheximide for 16 hours unless otherwise indicated. RNA was isolated using the RNeasy Mini Kit (Qiagen) and cDNA was generated using the Superscript III kit (ThermoFisher Scientific). Taqman quantitative PCR probes (Applied Biosystems) were used in conjunction with Taqman Master Mix (Applied Biosystems) to assess transcript levels for the following genes: *GAPDH* (Hs02786624_g1; VIC-MGB), *IL7Rα* (Hs00902334_m1; FAM-MGB), *BCL2L11* (Hs00708019_s1; FAM-MGB), *BCL2* (Hs00608023_m1; FAM-MGB), *FKBP5* (Hs01561006_m1; FAM-MGB), *GILZ* (Hs00608272_m1; FAM-MGB), *NR3C1* (H200353740_m1; FAM-MGB), *MYC* (Hs00153408_m1; FAM-MGB), and *ARHGEF3* (Hs00989814_m1; FAM-MGB). Experiments were performed in technical triplicate and were run on a QuantStudio 5 Real-Time PCR Instrument (Applied Biosystems). The fold change in transcript expression was calculated relative to cells treated with vehicle control using the delta-delta Ct method, unless otherwise indicated, with the use of *GAPDH* transcript for normalization.

Measurement of cell surface IL7Rα

For analysis of cell surface IL7Rα expression, cells were treated with 1μM DEX for 24 hours. Murine thymocyte experiments were performed in the presence of 100pg/mL recombinant murine IL7. Antibodies against human (BioLegend; 351315) or murine (Tonbo Biosciences; 20-1271) IL7Rα were used in conjunction with Hoechst 33258 to allow for gating on viable cells. Data are presented as the median fluorescent intensity (MFI) of the IL7Rα signal.

Cytokine stimulation and intracellular flow cytometry

Phosphoflow cytometry for measurement of STAT protein phosphorylation following IL7 stimulation was performed as previously described (14). Briefly, CCRF-CEM cells were exposed to vehicle control or 1μM DEX for 24 hours, allowed to rest for one hour in serum free media, and stimulated with IL7 at a concentration of 100ng/mL for 15 minutes. PDX cells were similarly allowed to rest in serum free media for one hour followed by stimulation with 100ng/mL IL7 for 15 minutes. Cells were subsequently fixed with 2% paraformaldehyde and permeabilized with methanol. STAT protein phosphorylation was assessed using antibodies against pSTAT1 pY701 (BD Biosciences; BDB612564), pSTAT3 pY705 (BD Biosciences; BDB612569), pSTAT5 pY694 (BD Biosciences; BDB612599), and pSTAT6 pY641 (BD Biosciences; BDB612601). BIM and BCL-2 protein expression were assessed following cell fixation and permeabilization using antibodies against BIM (Cell Signaling Technology; 2933) and anti-human (Life Technologies; A15796) or anti-mouse (BioLegend; 633509) BCL-2. GR expression was assessed using an anti-GR antibody. A donkey anti-rabbit secondary antibody (Jackson ImmunoResearch Laboratories) was used for flow cytometric detection of BIM and GR protein.

Luciferase reporter assay

CCRF-CEM cells were transiently transfected with the pGL4.52[*luc2P/*STAT5 RE/hygro] vector (Promega; E4651) using the Lipofectamine 3000 Transfection Reagent (Life Technologies). Eighteen

hours after transfection, cells were treated in the absence or presence of 1μM DEX, 100ng/mL recombinant human IL7, and/or 500nM ruxolitinib for 36 hours. Luciferase activity was assessed with the ONE-Glo Luciferase Assay System (Promega) and a Biotek Synergy 2 instrument. Relative luminescence was calculated by normalizing values to those obtained from cells treated with vehicle control.

RNA-seq analysis

Scramble control and STAT5 knockout CCRF-CEM cell clones were cultured in vehicle control or in the presence or absence of 1μM DEX and/or 100ng/mL recombinant human IL7 for 4 or 16 hours. RNA was isolated using the RNeasy Mini Kit and cDNA was generated using the Superscript III kit and quantified using a NanoDrop spectrophotometer (ThermoFisher). RNA quality was assessed using an Agilent Bioanalyzer (Agilent Technologies). Libraries were prepared using 1ng of RNA and were sequenced on the HiSeq 2500 (Illumina) to generate 50bp single end reads.

GR regulated genes were identified using edgeR, as previously described (35), by comparing scramble control clones treated with vehicle to those treated with DEX for four hours. A gene set was created using the statistical thresholds of absolute log fold change >1 and false discovery rate (FDR) <0.05. This analysis was then applied to perform the same comparison between scramble control clones treated with vehicle versus DEX plus IL7 for four hours. For the analysis of STAT5 target genes, gene set enrichment analysis (GSEA) was performed as previously described (36) by comparing scramble control clones treated with IL7 versus DEX plus IL7 using gene sets derived from published STAT5 ChIP-seq experiments in human CD4+ T-cells (23). The default settings were used for GSEA, including permutation based on phenotype. These data have been deposited in NCBI's Gene Expression Omnibus and are accessible through GEO Series accession number GSE137893.

For the fresh diagnostic T-ALL samples, total RNA was prepared using Trizol (ThermoFisher) based extraction. Samples were purified and concentrated using the RNeasy Mini or RNeasy MinElute Kit alone with the DNase Set (Qiagen). RNA concentration was determined using a NanoDrop spectrophotometer. RNA quality was assessed using an Agilent 2200 TapeStation (Agilent

Technologies). 100ng of RNA was used to prepare libraries using the TruSeq RNA Exome RNA kit (Illumina). For RNA samples with DV_{200} below 30%, 200ng of total RNA was used to prepare libraries. Libraries were sequenced on a NextSeq 500 using 150bp paired-end chemistry.

Primary T-ALL cell transcript expression was calculated via a local software pipeline built around the Bowtie 2 Aligner (v2.3.4.1) and RSEM's (v1.2.3.0) expectation-maximization quantification that utilized the Ensembl GRCh38 release 85 reference. After demultiplexing, converting primary sequence data to fastq format, and trimming adapters, sequences were aligned against an HG38 rRNA reference using the bwa (v0.7.12) aligner in order to screen out rRNA. Only non-rRNA aligning sequences advanced into the Bowtie 2/RSEM analysis stream. These data were used to generate gene signatures associated with early versus late thymocyte development via hierarchical clustering and dendrogram analysis.

All sequencing analysis, including read alignment, quality and performance metrics, post-processing, variant calling, and variant annotation were performed as previously described (37, 38) using the hg38 build of the human genome. Briefly, reads were aligned with Burrows-Wheeler Aligner (39) and processed using Picard (http://broadinstitute.github.io/picard) and the Genome Analysis Toolkit (GATK) (40) to perform base quality recalibration and multiple sequence realignment. Single nucleotide variants and indels were detected with the MuTect (41) and BCFtools algorithms, respectively. Variants were negatively selected against based on IGSR SNP (42) and ExAC SNP (43) databases and positively selected for based on recurrently mutated sites or regions within COSMIC (Acute T Lymphoblastic Leukemia associated subset of mutations) (44) or as previously reported (1). Candidate somatic mutations were manually reviewed using Integrative Genomics Viewer (45). These data have been deposited in NCBI's Gene Expression Omnibus and are accessible through GEO Series accession number GSE137768.

BH3 profiling

BH3 profiling was performed according to established methods (46). CCRF-CEM cells were treated with or without 1μM DEX and/or 100ng/mL recombinant human IL7 for 16 hours prior to

552 analysis. Thymocyte BH3 profiling was performed immediately after harvesting thymocytes.
553 Cytochrome c staining was performed using an anti-cytochrome c antibody (BioLegend; 612310).
554
555 **shRNA-mediated knockdown of *BCL2* and *ARHGEF3***
556 The miR30-PGK-NeoR-IRES-GFP cassette from LMN-GFP (32) was cloned into a pCDH
557 Expression Lentivector (System Biosciences) to generate the construct pCDH-LMN-GFP. Short hairpin
558 RNA (shRNA) sequences targeting human *BCL2* are as follows: shBCL2-1 – 5'-
559 TTTTATTCCAATTCCTTTCGGA-3'; shBCL2-2 – 5'-TAGCTGATTTGAAACTTCCCAA-3'; shBCL2-3
560 – 5'-TACTTCATCACTATCTCCCGGT-3'; shBCL2-4 – 5'-TTTAAGTACAGCATGATCCTCT-3';
561 and shBCL2-5 – 5'-TATCAGTCTACTTCCTCTGTGA-3'. shRNA sequences targeting human
562 *ARHGEF3* are as follows: shARHGEF3-1 – 5'-TTTGATTCAACTCTTGTTCTGT-3'; shARHGEF3-2 –
563 TATATCTTGTCACACAGCTTGA-3'; shARGHEF3-3 – TATAGCTTCTTCCAAGTGCTGC-3'. 97-mer
564 oligonucleotides were generated as previously described (47) and amplified using the following primers:
565 forward – 5'- TACAATACTCGAGAAGGTATATTGCTGTTGACAGTGAGCG-3'; reverse –
566 ACTTAGAAGAATTCCGAGGCAGTAGGCA-3'. A non-targeting shRNA (shControl) sequence was
567 used as a control: 5'-TAGATAAGCATTATAATTCCTA-3'. Oligonucleotides were cloned into the EcoRI
568 and XhoI sites of pCDH-LMN-GFP and lentivirus was generated via calcium phosphate transfection of
569 HEK293T cells using the packaging and envelope plasmids psPAX2 and pCMV-VSVG. Viral
570 supernatants were collected 48 hours after transfection and concentrated using Lenti-X Concentrator
571 (Clontech). Following lentiviral transduction, GFP positive cells were sorted using a Sony SH800
572 instrument and subsequently expanded.
573
574 **Flow cytometry**
575 Flow cytometry was performed using a BD FACSVerse and data were analyzed using FlowJo software.
576
577 **Statistics**

Statistical analyses were performed using Prism 8 (GraphPad). All tests were two-sided and the threshold for significance was $p \leq 0.05$. Comparisons between groups were made using t-tests, with one-way ANOVA and Tukey's method for multiple comparisons adjustment for comparisons of three or more groups. For in vivo survival analysis, the log-rank test was used to perform pairwise comparisons between survival curves. Interactions between drugs were assessed using Bliss independence analysis (48). Error bars represent the standard error of the mean.

Study Approval

Written informed consent for the use of diagnostic specimens for research was obtained from patients or their guardians at the time of sample collection, according to the Declaration of Helsinki, the National Cancer Institute, and institutional review boards of participating sites. All animal experiments were conducted following protocols that were approved by the Institutional Animal Care and Use Committees and Institutional Review Boards of Children's Hospital of Philadelphia or the University of California, San Francisco.

Author contributions

L.K.M., B.J.H., C.D.-M., K.M.S., D.T.T., and M.L.H. designed the experiments and analyzed the data. L.K.M., C.D.-M., B.J.H., A.M.W., and T.L.V. performed the experiments. B.L.W. performed immunophenotyping of patient samples. P.F. performed the RNA-sequencing of the primary patient samples. B.J.H., R.P.R., A.H., and A.B.O. performed bioinformatics analysis. L.K.M. and M.L.H. wrote the manuscript. B.J.H., C.D.-M., R.P.R., A.H., A.M.W., T.L.V., P.F., A.B.O., B.L.W., T.M.H., K.M.S., and D.T.T. reviewed the manuscript.

Acknowledgements

The authors thank Michael Adkisson, Joshua Rudolph, Andrea Barczak, and David Erle from the UCSF Functional Genomics Core Facility for their assistance with the RNA-seq involving CCRF-CEM cells and Anthony Letai and Jeremy Ryan for assistance with the BH3 profiling technique. This study was supported by a Genentech Foundation Research Fellowship (L.K.M.), National Institutes of Health Medical Scientist Training Program Grant T32GM007618 (L.K.M.), National Cancer Institute Grant R01CA193776 (T.M.H., B.L.W., D.T.T., and M.L.H.), American Cancer Society Research Scholar Grant RSG-13-022-01-CDD (D.T.T.), a Buster Posey Family Pediatric Cancer Pilot Award (M.L.H.), the Campini Family Foundation (M.L.H.), and the Pepp Family Foundation (M.L.H.). R.P.R., A.H., and A.B.O. are supported by the UCSF Helen Diller Family Comprehensive Cancer Center National Institutes of Health grant P30CA082103, which also supports the shared resource facilities that were used to conduct the flow cytometry work at UCSF. In addition, this work was supported by the NCTN Operations Center Grant U10CA180886 and NCTN Statistics and Data Center Grant U10CA180899 to the Children's Oncology Group (COG).

References

1. Liu Y et al. The genomic landscape of pediatric and young adult T-lineage acute lymphoblastic leukemia [Internet]. *Nat Genet* 2017;advance online publication.http://dx.doi.org/10.1038/ng.3909. cited

2. Pui C-H, Carroll WL, Meshinchi S, Arceci RJ. Biology, risk stratification, and therapy of pediatric acute leukemias: an update. *J. Clin. Oncol. Off. J. Am. Soc. Clin. Oncol.* 2011;29(5):551–565.

3. Bhojwani D, Pui C-H. Relapsed childhood acute lymphoblastic leukaemia. *Lancet Oncol.* 2013;14(6):e205-217.

4. Gao J, Liu W-J. Prognostic value of the response to prednisone for children with acute lymphoblastic leukemia: a meta-analysis. *Eur. Rev. Med. Pharmacol. Sci.* 2018;22(22):7858–7866.

5. Lauten M et al. Prediction of outcome by early bone marrow response in childhood acute lymphoblastic leukemia treated in the ALL-BFM 95 trial: differential effects in precursor B-cell and T-cell leukemia. *Haematologica* 2012;97(7):1048–1056.

6. Schmidt S et al. Glucocorticoid-induced apoptosis and glucocorticoid resistance: molecular mechanisms and clinical relevance. *Cell Death Differ.* 2004;11 Suppl 1:S45-55.

7. Erlacher M et al. TCR signaling inhibits glucocorticoid-induced apoptosis in murine thymocytes depending on the stage of development. *Eur. J. Immunol.* 2005;35(11):3287–3296.

8. Jamieson CA, Yamamoto KR. Crosstalk pathway for inhibition of glucocorticoid-induced apoptosis by T cell receptor signaling. *Proc. Natl. Acad. Sci. U. S. A.* 2000;97(13):7319–7324.

9. Tsitoura DC, Rothman PB. Enhancement of MEK/ERK signaling promotes glucocorticoid resistance in CD4+ T cells. *J. Clin. Invest.* 2004;113(4):619–627.

10. Spits H. Development of alphabeta T cells in the human thymus. *Nat. Rev. Immunol.* 2002;2(10):760–772.

644 11. Ribeiro D et al. STAT5 is essential for IL-7-mediated viability, growth, and proliferation of T-cell
645 acute lymphoblastic leukemia cells. *Blood Adv.* 2018;2(17):2199–2213.

646 12. Silva A et al. IL-7 contributes to the progression of human T-cell acute lymphoblastic leukemias.
647 *Cancer Res.* 2011;71(14):4780–4789.

648 13. Treanor LM et al. Interleukin-7 receptor mutants initiate early T cell precursor leukemia in murine
649 thymocyte progenitors with multipotent potential. *J. Exp. Med.* 2014;211(4):701–713.

650 14. Delgado-Martin C et al. JAK/STAT pathway inhibition overcomes IL7-induced glucocorticoid
651 resistance in a subset of human T-cell acute lymphoblastic leukemias. *Leukemia* [published online
652 ahead of print: May 9, 2017]; doi:10.1038/leu.2017.136

653 15. Mazzucchelli R, Durum SK. Interleukin-7 receptor expression: intelligent design. *Nat. Rev. Immunol.*
654 2007;7(2):144–154.

655 16. Chen W et al. Glucocorticoid receptor phosphorylation differentially affects target gene expression.
656 *Mol. Endocrinol. Baltim. Md* 2008;22(8):1754–1766.

657 17. Abe A et al. An Enhancer of the IL-7 Receptor α-Chain Locus Controls IL-7 Receptor Expression
658 and Maintenance of Peripheral T Cells. *J. Immunol. Baltim. Md 1950* 2015;195(7):3129–3138.

659 18. Franchimont D et al. Positive effects of glucocorticoids on T cell function by up-regulation of IL-7
660 receptor alpha. *J. Immunol. Baltim. Md 1950* 2002;168(5):2212–2218.

661 19. Kakal JA et al. Transcriptional regulation of the IL-7Rα gene by dexamethasone and IL-7 in primary
662 human CD8 T cells. *Immunogenetics* 2017;69(1):13–27.

663 20. Shimba A et al. Glucocorticoids Drive Diurnal Oscillations in T Cell Distribution and Responses by
664 Inducing Interleukin-7 Receptor and CXCR4. *Immunity* 2018;48(2):286-298.e6.

21. Lee H-C, Shibata H, Ogawa S, Maki K, Ikuta K. Transcriptional regulation of the mouse IL-7 receptor alpha promoter by glucocorticoid receptor. *J. Immunol. Baltim. Md 1950* 2005;174(12):7800–7806.

22. Kruth KA et al. Suppression of B-cell development genes is key to glucocorticoid efficacy in treatment of acute lymphoblastic leukemia. *Blood* 2017;129(22):3000–3008.

23. Kanai T et al. Identification of STAT5A and STAT5B target genes in human T cells. *PloS One* 2014;9(1):e86790.

24. Jing D et al. Opposing regulation of BIM and BCL2 controls glucocorticoid-induced apoptosis of pediatric acute lymphoblastic leukemia cells. *Blood* 2015;125(2):273–283.

25. Berki T, Pálinkás L, Boldizsár F, Németh P. Glucocorticoid (GC) sensitivity and GC receptor expression differ in thymocyte subpopulations. *Int. Immunol.* 2002;14(5):463–469.

26. Boldizsár F et al. Low glucocorticoid receptor (GR), high Dig2 and low Bcl-2 expression in double positive thymocytes of BALB/c mice indicates their endogenous glucocorticoid hormone exposure. *Immunobiology* 2006;211(10):785–796.

27. Gruber J, Sgonc R, Hu YH, Beug H, Wick G. Thymocyte apoptosis induced by elevated endogenous corticosterone levels. *Eur. J. Immunol.* 1994;24(5):1115–1121.

28. Lee MS, Hanspers K, Barker CS, Korn AP, McCune JM. Gene expression profiles during human CD4+ T cell differentiation. *Int. Immunol.* 2004;16(8):1109–1124.

29. Foo J, Michor F. Evolution of acquired resistance to anti-cancer therapy. *J. Theor. Biol.* 2014;355:10–20.

30. Pieters R et al. Relation of cellular drug resistance to long-term clinical outcome in childhood acute lymphoblastic leukaemia. *Lancet Lond. Engl.* 1991;338(8764):399–403.

687 31. Inaba H, Pui C-H. Glucocorticoid use in acute lymphoblastic leukaemia. *Lancet Oncol.*
688 2010;11(11):1096–1106.

689 32. Doench JG et al. Optimized sgRNA design to maximize activity and minimize off-target effects of
690 CRISPR-Cas9. *Nat. Biotechnol.* 2016;34(2):184–191.

691 33. Schumann K et al. Generation of knock-in primary human T cells using Cas9 ribonucleoproteins.
692 *Proc. Natl. Acad. Sci. U. S. A.* 2015;112(33):10437–10442.

693 34. Brinkman EK, Chen T, Amendola M, van Steensel B. Easy quantitative assessment of genome
694 editing by sequence trace decomposition. *Nucleic Acids Res.* 2014;42(22):e168.

695 35. Robinson MD, McCarthy DJ, Smyth GK. edgeR: a Bioconductor package for differential expression
696 analysis of digital gene expression data. *Bioinforma. Oxf. Engl.* 2010;26(1):139–140.

697 36. Subramanian A et al. Gene set enrichment analysis: a knowledge-based approach for interpreting
698 genome-wide expression profiles. *Proc. Natl. Acad. Sci. U. S. A.* 2005;102(43):15545–15550.

699 37. Iyer G et al. Genome sequencing identifies a basis for everolimus sensitivity. *Science*
700 2012;338(6104):221.

701 38. Al-Ahmadie H et al. Synthetic lethality in ATM-deficient RAD50-mutant tumors underlies outlier
702 response to cancer therapy. *Cancer Discov.* 2014;4(9):1014–1021.

703 39. Li H, Durbin R. Fast and accurate short read alignment with Burrows-Wheeler transform.
704 *Bioinforma. Oxf. Engl.* 2009;25(14):1754–1760.

705 40. DePristo MA et al. A framework for variation discovery and genotyping using next-generation DNA
706 sequencing data. *Nat. Genet.* 2011;43(5):491–498.

707 41. Cibulskis K et al. Sensitive detection of somatic point mutations in impure and heterogeneous
708 cancer samples. *Nat. Biotechnol.* 2013;31(3):213–219.

709 42. Clarke L et al. The international Genome sample resource (IGSR): A worldwide collection of
710 genome variation incorporating the 1000 Genomes Project data. *Nucleic Acids Res.*
711 2017;45(D1):D854–D859.

712 43. Lek M et al. Analysis of protein-coding genetic variation in 60,706 humans. *Nature*
713 2016;536(7616):285–291.

714 44. Tate JG et al. COSMIC: the Catalogue Of Somatic Mutations In Cancer. *Nucleic Acids Res.*
715 2019;47(D1):D941–D947.

716 45. Robinson JT et al. Integrative genomics viewer. *Nat. Biotechnol.* 2011;29(1):24–26.

717 46. Ryan J, Letai A. BH3 profiling in whole cells by fluorimeter or FACS. *Methods San Diego Calif*
718 2013;61(2):156–164.

719 47. Fellmann C et al. An optimized microRNA backbone for effective single-copy RNAi. *Cell Rep.*
720 2013;5(6):1704–1713.

721 48. Zhao W et al. A New Bliss Independence Model to Analyze Drug Combination Data. *J. Biomol.*
722 *Screen.* 2014;19(5):817–821.

723

724

725

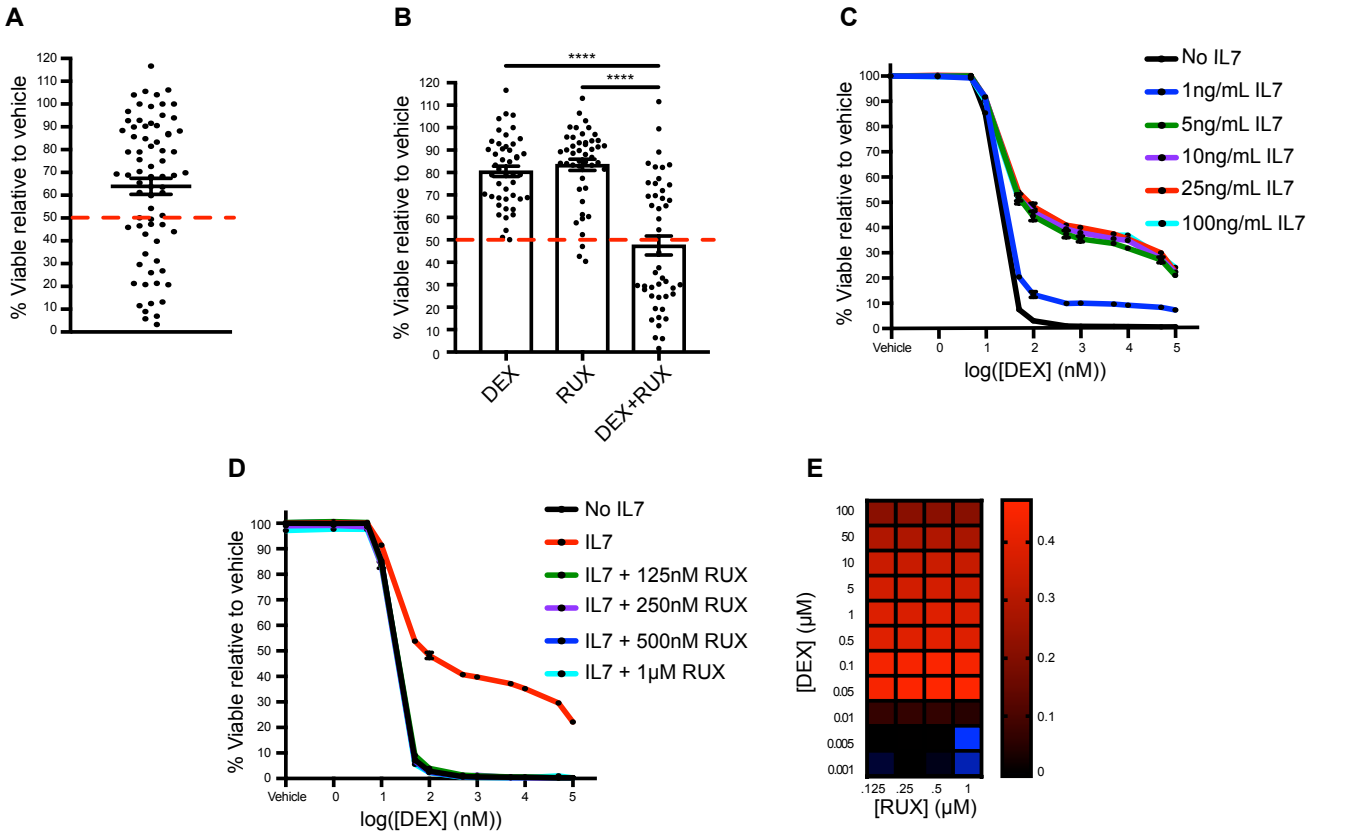

Fig. 1. JAK/STAT inhibition overcomes DEX resistance in a subset of primary T-ALL samples and in the T-ALL cell line CCRF-CEM. (A) Viability relative to vehicle control of cells from 73 primary diagnostic T-ALL samples exposed to 2.5μM DEX for 48 hours in the presence of 25ng/mL IL7. The red line indicates the 50% viability cutoff used to define "DEX resistant". **(B)** Viability relative to vehicle control of cells from the 46 DEX resistant primary diagnostic T-ALL samples in (A) exposed to 2.5μM DEX and/or 0.5μM RUX for 48 hours in the presence of 25ng/mL IL7. Statistical significance was assessed using one-way ANOVA with Tukey's method for multiple comparisons adjustment. **(C)** Viability of CCRF-CEM cells exposed to DEX in the absence or presence of increasing concentrations of IL7 for 72 hours in technical triplicate. **(D)** Viability of CCRF-CEM cells exposed to DEX in the presence of 25ng/mL IL7 in the absence or presence of increasing concentrations of RUX in technical triplicate. The no IL7 (black line) and the 25ng/mL IL7 (red line) conditions are re-plotted from figure 1C. **(E)** Heatmap of Bliss independence scores calculated as the average of technical triplicates for the combination of DEX and RUX in CCRF-CEM cells cultured in the presence of 25ng/mL IL7 for 72 hours, in which positive values, indicated in red, are indicative of a synergistic interaction. All CCRF-CEM cell data are representative of three independent experiments. ****p<0.0001, ***p<0.001, **p<0.01, *p<0.05.

Figure 2

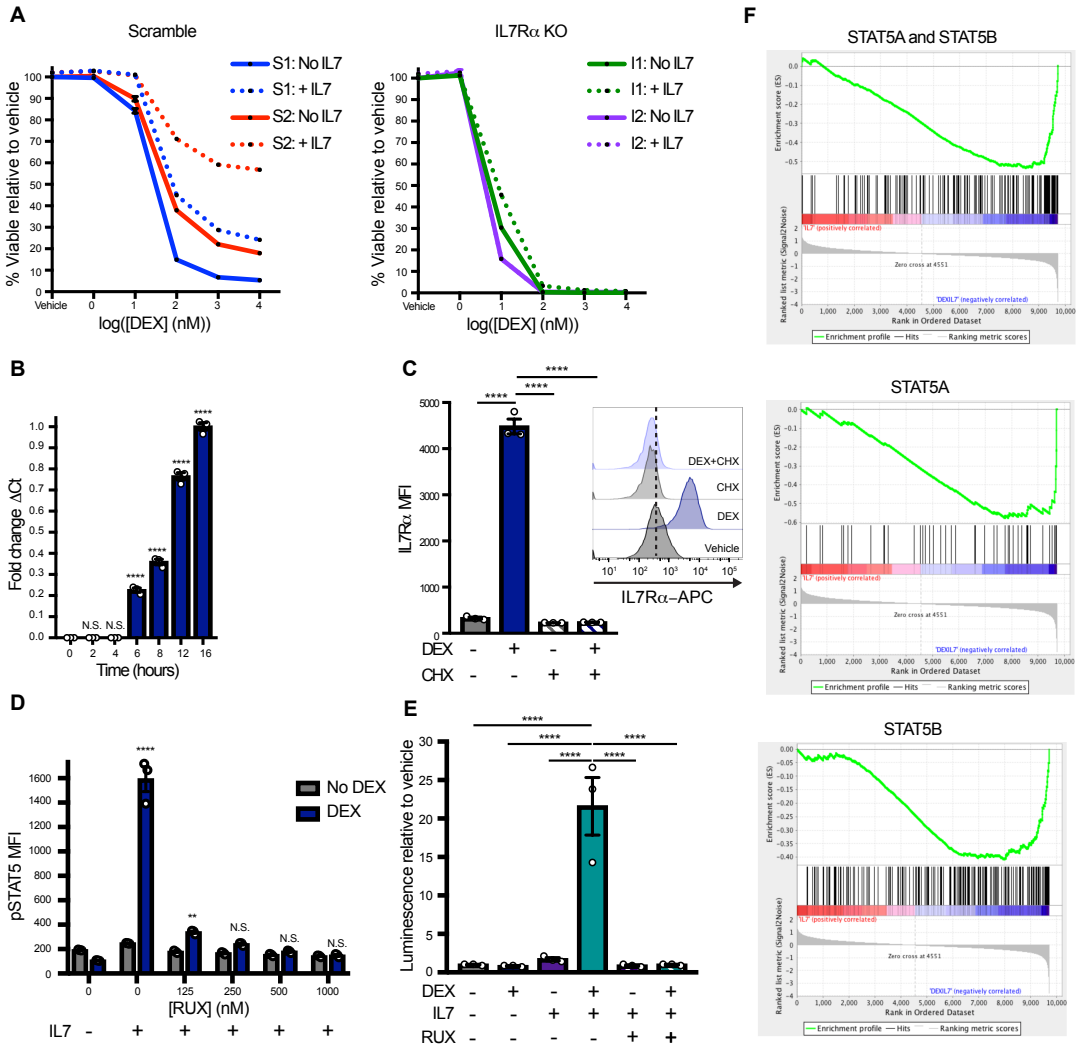

Fig. 2. DEX exposure augments IL7R expression and downstream JAK/STAT signaling. (A) Viability of scramble control (S1 and S2; left) and IL7Rα KO (I1 and I2; right) CCRF-CEM cell clones exposed to DEX in the absence (solid lines) or presence (dotted lines) of 25ng/mL IL7 in technical triplicate for 72 hours. **(B)** Fold change relative to the 16 hour time point of the ΔCt of *IL7RA* transcript relative to *GAPDH* as determined by qPCR performed in technical triplicate in CCRF-CEM cells exposed to 1μM DEX and 100ng/mL IL7 for the indicated period of time. **(C)** MFI of IL7Rα in CCRF-CEM cells treated with or without 1μM DEX and/or 10μg/mL CHX in technical triplicate for 24 hours. Inset shows representative histograms of IL7Rα in CCRF-CEM cells treated with or without 1μM DEX and/or 10μg/mL CHX for 24 hours. **(D)** MFI of pSTAT5 in CCRF-CEM cells treated with or without 1μM DEX for 24 hours in the absence of IL7 followed by a one-hour exposure to vehicle control or RUX prior to a 15-minute stimulation with 100ng/mL IL7 in technical triplicate. Significance is relative to the DEX-treated condition in the absence of IL7 stimulation. **(E)** Relative luminescence of CCRF-CEM cells transfected with the STAT5 reporter construct and treated with or without 1μM DEX, 100ng/mL IL7, and 500nM RUX in technical triplicate for 36 hours prior to lysis and measurement of luciferase activity. **(F)** GSEA plots of STAT5 gene expression signatures comparing scramble control clones (n=4) treated with 100ng/mL IL7 versus the combination of 1μM DEX and 100ng/mL IL7 for 16 hours. Statistical significance was assessed using one-way ANOVA with Tukey's method for multiple comparisons adjustment (B-E). With the exception of the RNA-seq experiment, all data are representative of three independent experiments. ****p<0.0001, ***p<0.001, **p<0.01, *p<0.05, N.S. – not significant.

Figure 3

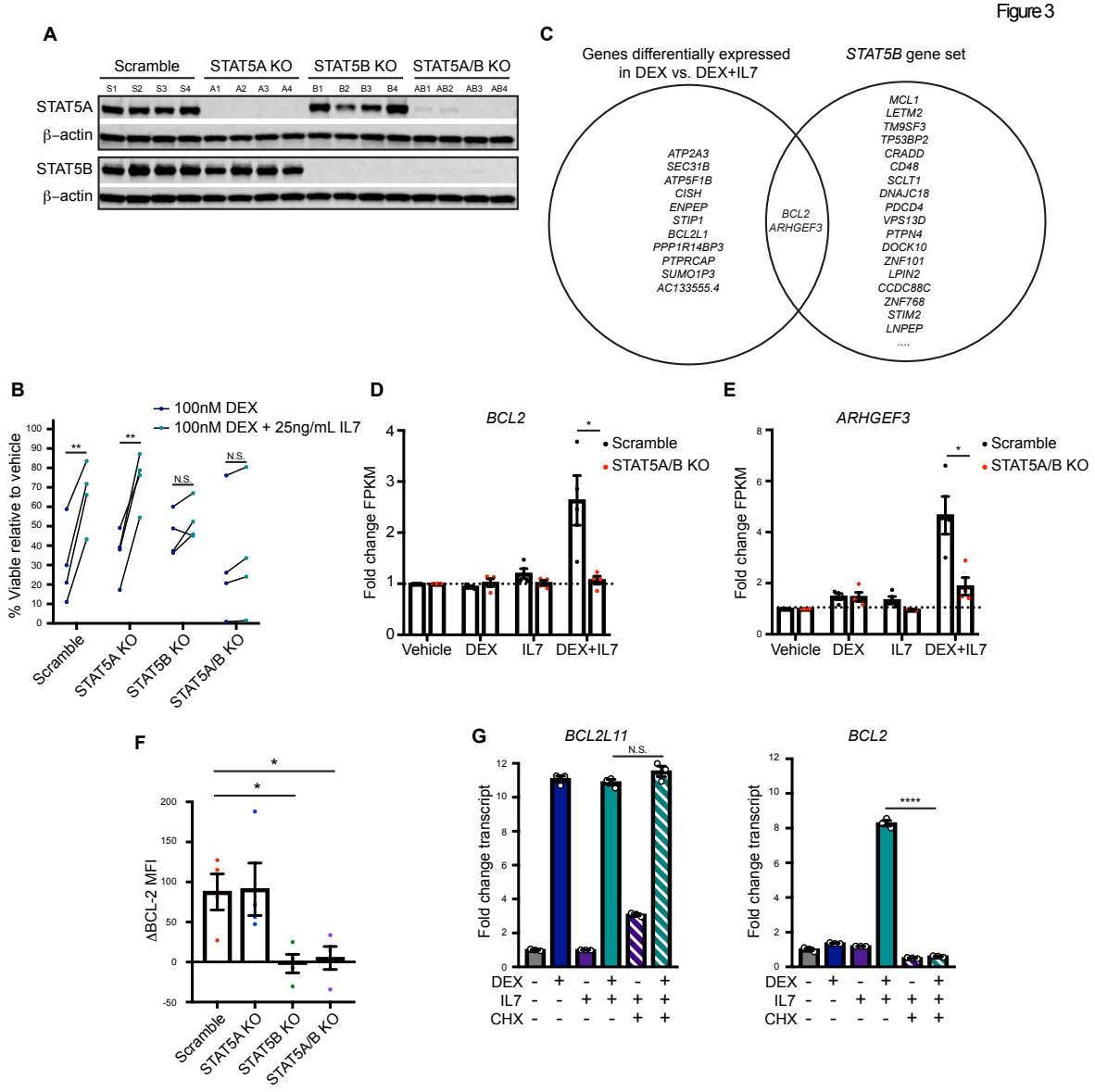

Fig. 3. STAT5B, but not STAT5A, mediates the upregulation of BCL-2 expression in cells exposed to the combination of DEX and IL7. (A) Evaluation of STAT5A and STAT5B expression by Western blot in independent scramble control (S) and STAT5 single (A or B) and double (AB) KO CCRF-CEM cell clones (n=4 per genotype). **(B)** Viability of independent scramble control and STAT5 KO CCRF-CEM cell clones (n=4 per genotype) treated with 100nM DEX with or without 25ng/mL IL7 for 72 hours. **(C)** Venn diagram depicting the overlap between the top differentially expressed genes between scramble control CCRF-CEM cell clones (n=4) treated with DEX versus DEX+IL7 and *STAT5B* target genes. **(D-E)** Fold change in the FPKM values for **(D)** *BCL2* transcript and **(E)** *ARHGEF3* transcript as determined by RNA-seq analysis of scramble control (n=4) and STAT5A/B double KO (n=4) CCRF-CEM cell clones treated in the absence or presence of 100ng/mL IL7 and/or 1μM DEX for 16 hours. **(F)** ΔMFI of BCL-2 protein expression in scramble control (n=4) and STAT5 KO (n=4) CCRF-CEM cell clones treated with 100ng/mL IL7 and 1μM DEX relative to 100ng/mL IL7 alone for 48 hours. **(G)** *BCL2L11* and *BCL2* transcript expression in CCRF-CEM cells cultured in the absence or presence of 1μM DEX, 100ng/mL IL7, and/or 10μg/mL CHX for 16 hours as determined by qPCR performed in technical triplicate. Statistical significance was assessed using a paired t-test (B), two-sample t-tests (D and E), or one-way ANOVA with Tukey's method for multiple comparisons adjustment (F and G). With the exception of the RNA-seq experiment, all data are representative of three independent experiments. ****p<0.0001, ***p<0.001, **p<0.01, *p<0.05, N.S. – not significant.

Figure 4

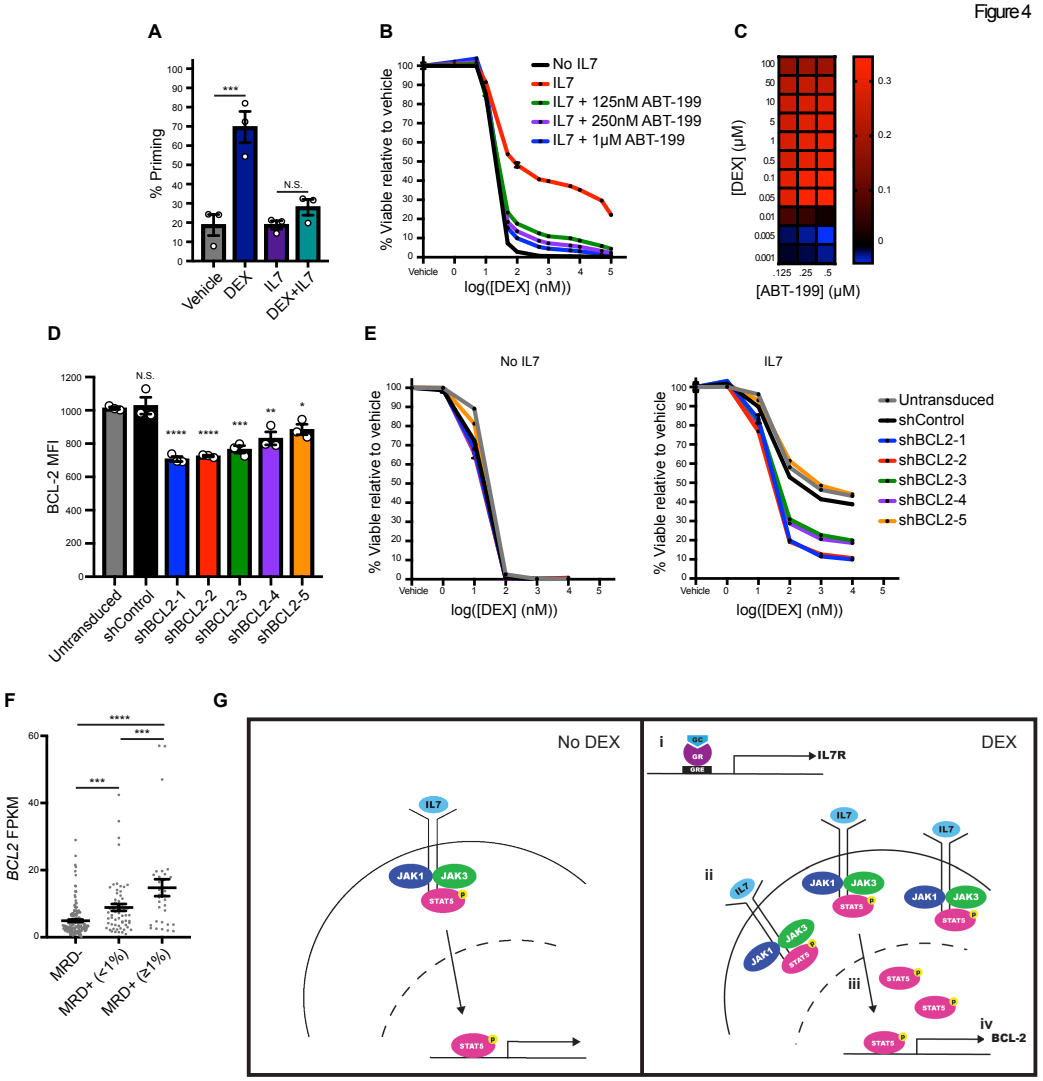

Fig. 4. BCL-2 mediates IL7-induced DEX resistance. (A) Percent priming of CCRF-CEM cells treated in the absence or presence of 1μM DEX and/or 100ng/mL IL7 in technical triplicate for 16 hours followed by BH3 profiling with 0.5μM ABT-199 for 90 minutes. **(B)** Viability of CCRF-CEM cells treated with DEX in the absence or presence of 25ng/mL IL7 and increasing concentrations of ABT-199 for 72 hours in technical triplicate. The no IL7 (black line) and the 25ng/mL IL7 (red line) conditions are re-plotted from figure 1C. **(C)** Heatmap of Bliss independence scores calculated as the average of technical triplicates for the combination of DEX and ABT-199 in the presence of 25ng/mL IL7. **(D)** MFI of BCL-2 protein expression assessed in technical triplicate in untransduced CCRF-CEM cells and CCRF-CEM cells transduced with a non-targeting shRNA control (shControl) or a *BCL2*-targeting shRNA (shBCL2-1-5). Statistical significance is relative to the untransduced cells. **(E)** Viability of untransduced or shRNA-transduced CCRF-CEM cells treated with DEX in the absence (left) or presence (right) of 25ng/mL IL7 in technical triplicate for 72 hours. **(F)** FPKM values for *BCL2* transcript obtained from published RNA-seq data from diagnostic samples from patients enrolled on COG AALL0434, stratified based on day 29 bone marrow MRD. **(G)** Schematic of the proposed model for the mechanism by which DEX paradoxically induces steroid resistance in T-ALL cells in the presence of IL7. In the presence of DEX (right), GR induces an increase in IL7R expression (i) leading to an increase in IL7R at the cell surface (ii). This in turn leads to an increase in STAT5 transcriptional activity (iii) that ultimately results in the upregulation of BCL-2 (iv). Statistical significance was assessed using one-way ANOVA with Tukey's method for multiple comparisons adjustment (A, D, and F). All CCRF-CEM cell data are representative of three independent experiments. ****p<0.0001, ***p<0.001, **p<0.01, *p<0.05, N.S. – not significant.

Figure 5

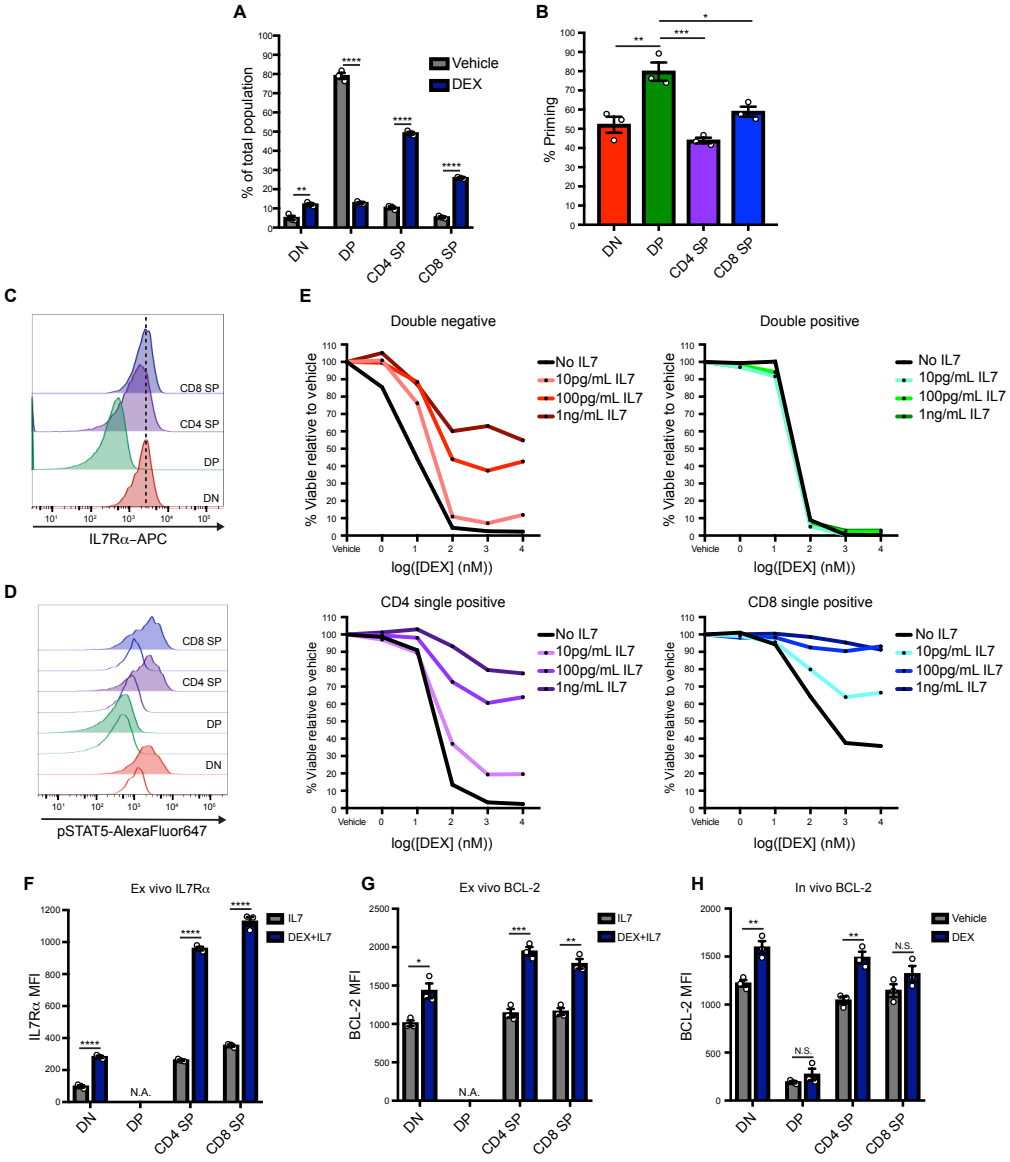

Fig. 5. IL7 induces DEX resistance in subpopulations of normal developing thymocytes. (A) Percentage of thymocyte subpopulations in thymi isolated from mice treated with vehicle control (n=3) or DEX (n=3) at 2mg/kg/day for three days. **(B)** Percent priming of thymocytes in the basal state following BH3 profiling with 1μM synthetic BIM peptide in technical triplicate for 90 minutes. **(C)** Histograms of the basal expression of IL7Rα in the major murine thymocyte subpopulations. **(D)** Histograms of pSTAT5 in the major murine thymocyte subpopulations in the basal state (unfilled histograms) and following a 15-minute stimulation with 100ng/mL IL7 (filled histograms). **(E)** Viability of murine thymocyte subpopulations following ex vivo treatment for 24 hours with DEX in the absence or presence of increasing concentrations of IL7. **(F)** MFI of IL7Rα in murine thymocytes treated ex vivo in the presence of 100pg/mL IL7 with or without 1μM DEX in technical triplicate for 24 hours. DP cells could not be analyzed due to lack of viable cells remaining after DEX exposure (not analyzed; N.A.). **(G)** MFI of BCL-2 in murine thymocytes treated ex vivo in the presence of 100pg/mL IL7 with or without 1μM DEX in technical triplicate for 24 hours. DP cells could not be analyzed due to lack of viable cells remaining after DEX exposure (N.A.). **(H)** MFI of BCL-2 in thymocytes isolated from mice treated with vehicle control (n=3) or DEX (n=3) at 2mg/kg/day for three days. Statistical significance was assessed using two-sample t-tests (A, F, G, and H) or one-way ANOVA with Tukey's method for multiple comparisons adjustment (B). All data are representative of three independent experiments. ****p<0.0001, ***p<0.001, **p<0.01, *p<0.05, N.S. – not significant.

Figure 6

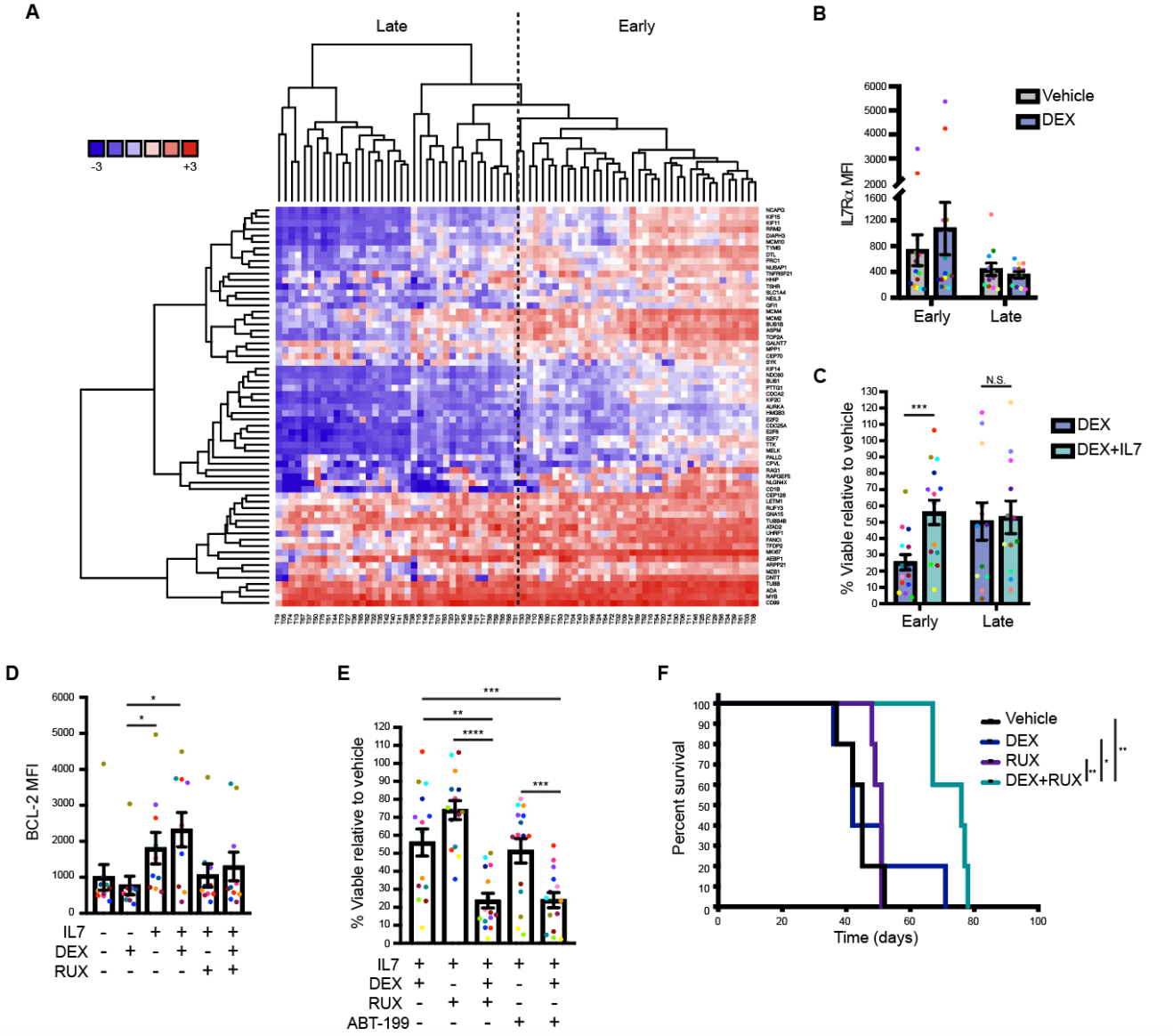

Fig. 6. T-ALLs reflecting early stages of T-cell development demonstrate DEX resistance in the presence of IL7. (A) Heatmap depicting the clustering of 76 primary T-ALL samples by expression of genes that are upregulated in early developing thymocytes relative to later developing thymocytes. **(B)** MFI of cell surface IL7Rα in 15 early and 12 late T-ALL PDX samples following exposure to 1μM DEX for 24 hours in technical triplicate. **(C)** Viability relative to vehicle control of 15 early and 12 late T-ALL PDX samples treated with 1μM DEX in the absence or presence of 25ng/mL IL7 for 48 hours in technical triplicate. **(D)** MFI of BCL-2 protein expression in 10 early T-ALL PDX samples following exposure to 100ng/mL IL7 with or without 1μM DEX and 500nM RUX for 16 hours in technical triplicate. Some samples were not analyzed due to limitations in cell numbers. **(E)** Viability relative to vehicle control of 15 early T-ALL samples exposed to 25ng/mL IL7 with or without 1μM DEX and/or 500nM RUX or 1μM ABT-199 for 48 hours in technical triplicate. **(F)** Kaplan-Meier survival analysis of mice transplanted with early T-ALL T24 and treated with vehicle control (n=5), DEX (n=5), RUX (n=5), or the combination of DEX and RUX (n=5). Statistical significance was assessed using paired t-tests (B and C), one-way ANOVA with Tukey's method for multiple comparisons adjustment (D and E), or a log-rank test (F). ****p<0.0001, ***p<0.001, **p<0.01, *p<0.05, N.S. – not significant.